Electrochimica Acta 530 (2025) 146390

Contents lists available at ScienceDirect

Electrochimica Acta

journal homepage: www.journals.elsevier.com/electrochimica-acta

Electrochemical degradation of levofloxacin in synthetic hospital effluents: insights into operating parameters, by-products formation and toxicity

Ana Hayat, José L.S. Duarte, Fermín Cruz-Gómez, Carmen M. Domínguez, Aurora Santos, Salvador Cotillas *

Department of Chemical and Materials Engineering, Faculty of Chemical Sciences, Complutense University of Madrid, Avenida Complutense s/n, 28040 Madrid, Spain

ARTICLE INFO

Keywords:
Levofloxacin
Electrochemical oxidation
Hospital effluents
BDD anode
RuO_2/Ti anode
Toxicity

ABSTRACT

This study investigates the electrochemical degradation of the broad-spectrum antibiotic levofloxacin (LVX) in synthetic hospital effluents using two different anode materials: Boron-Doped Diamond (BDD) and RuO_2/Ti. Experiments were performed under a range of current densities (5–50 mA cm^{-2}) to assess removal efficiency, reaction kinetics, intermediate by-product formation, and effluent toxicity. The degradation process was modelled using first-order kinetics, revealing that complete LVX removal is achievable under optimised operating conditions. BDD anodes demonstrated higher degradation efficiency at lower current densities, whereas RuO_2/Ti anodes required higher values to attain comparable degradation rates. Detailed analyses of electrogenerated oxidants and intermediate compounds indicated that direct oxidation at the anode surface and mediated oxidation via hydroxyl radicals and other reactive species contribute significantly to the degradation mechanism.

Additionally, the breakdown of organics in the effluent resulted in the release of nitrogen, primarily as nitrate, which is subsequently reduced to ammonium and further reacts with hypochlorite to form chloramines, thereby enhancing the degradation process, mainly when using RuO_2/Ti anodes. Mineralisation studies showed that Total Organic Carbon (TOC) removal exceeded 80 % with BDD anodes. Toxicity evaluations, conducted in vitro and silico methods, confirmed that most of the by-products generated during treatment pose minimal environmental risk. These findings underscore the potential of electrochemical oxidation as a sustainable and robust technology for the remediation of pharmaceutical contaminants in hospital effluents.

1. Introduction

Over the years, the continuous release of pollutants into the environment driven by industrialisation and evolving human lifestyles has increasingly pressured aquatic ecosystems [1–4]. Among various water contaminants, pharmaceutical residues, classified as emerging contaminants, pose a significant challenge due to their potential impacts on the environment and human health [5,6]. Hospitals rank among the largest consumers of pharmaceutical products and their metabolites, which include antibiotics, analgesics, antineoplastics and iodinated contrast agents. Since most of these drugs are not completely metabolised in the body, they are excreted through hospital effluents, which can range from 400 to 1200 dm^3 per bed per day, depending on the capacity of the healthcare facility [7]. When mixed with urban wastewater, these effluents are discharged into Wastewater Treatment Plants (WWTPs), which have demonstrated low efficiency in removing pharmaceutical compounds [8–11].

Antibiotics, particularly fluoroquinolones, have become increasingly common for treating infectious diseases, which account for approximately 25 % of global morbidity and mortality, according to the World Health Organization (WHO) [12–14]. Among these, levofloxacin (LVX) is a broad-spectrum antibiotic effective against Gram-positive and Gram-negative bacteria, and it is widely employed to treat severe bacterial and nosocomial infections [15]. After oral administration, up to 80 % of LVX is excreted unmetabolised [16]. Consequently, LVX concentrations in micrograms per litre to milligrams per litre have been detected in hospital effluents [17,18]. In contrast, levels in nanograms per litre to micrograms per litre have been observed in wastewater [19]. In this context, it is crucial to develop clean and efficient technologies to remove pharmaceutical compounds, especially antibiotics, from hospital effluents before their discharge into WWTPs [20].

Several Advanced Oxidation Processes (AOPs), such as ozonation,

* Corresponding author.
E-mail address: salvacot@ucm.es (S. Cotillas).

https://doi.org/10.1016/j.electacta.2025.146390
Received 28 February 2025; Received in revised form 17 April 2025; Accepted 3 May 2025
Available online 4 May 2025

photoelectrocatalysis, electro-Fenton or activated peroxymonosulfate, have been proposed to remove LVX, yielding promising results [21–25]. For instance, Goulart et al. investigated the degradation of LVX in synthetic urine by photoelectrolysis using an MMO electrode [22]. Their findings revealed that electrochemical oxidation at a low applied potential (0.2 V) was insufficient to degrade LVX, whereas photoelectrochemical oxidation using a Ti/MMO/ZnO photoanode achieved high removal efficiency. Similarly, Xue et al. examined the heterogeneous activation of peroxymonosulfate (PMS) for LVX degradation under various reaction conditions [24]. They demonstrated that efficient activation of PMS (50 mg dm^{-3}) by a catalyst (50 mg dm^{-3} MgO/Co_3O_4) resulted in the degradation of 96.93 % of an initial 10 mg dm^{-3} LVX solution. However, most studies have focused on removing LVX in simple matrices, which differ considerably from real effluents. Therefore, validating these results in real or complex matrices that closely mimic actual wastewater compositions is essential.

With this background, the present work evaluates the electrochemical oxidation of synthetic hospital effluents containing LVX as a fluoroquinolone antibiotic model. This technology has proven highly effective in removing recalcitrant organic compounds by generating non-selective $^{\bullet}OH$ radicals [26–29]. Consequently, it is considered one of the most promising approaches for eliminating pharmaceuticals from hospital effluents. This study will assess the influence of the anode material (Boron-Doped Diamond, (BDD) and RuO_2/Ti) and the current density (5–50 mA cm^{-2}) on the process performance. Additionally, the intermediate compounds formed during the electrochemical degradation of LVX will be analysed and identified to propose potential degradation pathways. Finally, the ecotoxicity of the treated samples will be evaluated using data from the Ecological Structure-Activity Relationship (ECOSAR) software, which predicts aquatic toxicity based on quantitative structure-activity relationships derived from both in vitro and *in silico* methods. In vitro assays involving organisms of varying complexity (bacteria, algae, daphnids, and fish) will be employed to assess acute and chronic toxicity effects [30].

2. Material and methods

2.1. Chemicals

Levofloxacin (LVX, $C_{18}H_{20}FN_3O_4$) of analytical grade (> 98 % purity) was obtained from Sigma-Aldrich. The synthetic hospital wastewater (HWW) was prepared using analytical grade reagents: sodium chloride, ammonium chloride, calcium chloride, sodium phosphate, sodium nitrate and sodium bicarbonate (Sigma Aldrich), magnesium sulphate and sodium acetate (Fisher), and urea, potassium sulphate and sodium sulphate (Panreac). Additional chemicals used for urea determination (4-(dimethylamino)benzaldehyde and hydrochloric acid) were of analytical grade and purchased from Sigma-Aldrich. Sulfuric acid, potassium iodide (Fischer), and a starch solution (Panreac) were employed to quantify total oxidants. The concentrations of anions were analysed using sodium carbonate (Panreac) and sodium bicarbonate (Sigma-Aldrich), while oxalic acid and nitric acid (Sigma-Aldrich) were used for cations analysis. HPLC-grade acetonitrile (Fischer) and formic acid (Sigma-Aldrich) were used as mobile phases during HPLC determinations.

2.2. Experimental procedure

A single-compartment electrochemical cell operating in batch mode was used for the electrochemical oxidation experiments [31]. Briefly, circular BDD ([B]: 500 mg dm^{-3}) and RuO_2/Ti electrodes, purchased from NeoCoat and Tianode, respectively, served as anodes, while a stainless-steel electrode was used as the cathode. The inter-electrode gap was 9 mm, and the total electrode surface area was 78 cm^2. The main features of the cell have been described in detail in previous works [32].

The synthetic HWW was prepared as an aqueous solution containing the organic and inorganic compounds listed in Table 1, as reported in the literature [33]. One litre of HWW spiked with 5 mg dm^{-3} LVX was transferred to a cylindrical borosilicate tank and pumped through the electrochemical cell at 440 mL min^{-1}. Electrochemical oxidation tests were conducted under galvanostatic conditions with current densities ranging from 5 to 50 mA cm^{-2}. These current densities were chosen based on promising results from previous studies, where low current densities effectively degraded other antibiotics, such as chloramphenicol [34]. The electric current was provided by a Dr Meter PS-3010DF DC power supply (0–30 V, 0–10A).

2.3. Analytical methods

A high-performance liquid chromatography (HPLC) system (Agilent 1100 series) with a DAD detector was employed to measure LVX concentration. An analytical column Poroshell 120 EC—C18 4 μm (4.6 × 150 mm) was used at 40 ºC. The mobile phase comprised 70 % formic acid (0.1 %) and 30 % acetonitrile, with a flow rate of 0.6 cm^3 min^{-1}, an injection volume of 20 μL and a DAD detection wavelength of 295 nm [35]. Urea concentration was determined using a colourimetric method described elsewhere [36,37]. Total Organic Carbon (TOC) was measured using a Shimadzu TOC-V CSH analyser, which performs oxidative combustion at 714 ºC with CO_2 detection via infrared spectroscopy.

Ion chromatography (IC) was employed to determine inorganic ions. Anions were measured using a Metrohm 930 Compact IC Flex equipped with a conductivity detector and a Metrosep A Supp 5 250/4.0 column, while cations were analysed using a Metrosep C6 250/4.0 column. The mobile phases used were Na_2CO_3 (3.2 μM) and $NaHCO_3$ (1 μM) at a flow rate of 0.7 cm^3 min^{-1} for anions, and oxalic acid (1 mM) and nitric acid (3 mM) at a flow rate of 1 cm^3 min^{-1} for cations. Each sample was injected at a volume of 20 μL. Oxidants were determined iodometrically using H_2SO_4 (20 %), KI and a starch solution (1 %), following the method described by Kolthoff & Carr [38]. Conductivity and pH were measured simultaneously using a HI5521 pH/EC Meter (Hanna Instruments).

The identification of LVX intermediates was performed using a high-resolution quadrupole time-of-flight mass spectrometer (QTOF Impact II, Bruker Daltonics, Billerica, MA) coupled to an Ultra-High-Performance Liquid Chromatography (UHPLC) system (ELUTE, Bruker Daltonics, Billerica, MA). Compounds were separated using a Bruker Intensity Solo HPLC Column C18 (2 μm particle size, 2 mm x 100 mm) and detected by an Electrospray ionisation (ESI, positive mode) with an Apollo II Ion source. The injection volume was 10 μL. The mobile phases were acetonitrile (A) and ultrapure water containing 0.1 % formic acid (B) at a flow rate of 0.4 cm^3 min^{-1}. The gradient started with 5 % B, increased to 95 % B over 10 min, was maintained at 95 % B until 12 min, returned to initial conditions at 13 min, and concluded at 15 min.

Table 1
Composition of synthetic hospital effluent.

Compound	Concentration (mg dm^{-3})
Cl^-	301.77
NO_3^-	5.11
PO_4^{3-}	14.48
SO_4^{2-}	70.60
NH_4^+	10.10
Na^+	351.03
Mg^{2+}	3.03
K^+	20.17
Ca^{2+}	5.05
HCO_3^-	50
CH_3COO^-	323.66
NH_2CONH_2 (urea)	375
COD	315
BOD_5	220
pH	7.5

Aquatic toxicity of the chemicals was predicted using ECOSAR for Windows (version 2.2), which estimates toxicity on structural similarities to compounds with known aquatic toxicity [39]. Acute and chronic toxicity were assessed for marine organisms, including fish, *Daphnia* and green algae.

3. Results and discussion

Fig. 1 shows the evolution of LVX concentration with the operation time during the electrochemical oxidation of synthetic hospital effluents polluted with 5 mg dm^{-3} LVX using BDD and RuO_2/Ti anodes at different current densities.

As can be observed, the LVX concentration decreases over time, regardless of the current density and the anode material used. However, these parameters influence the removal percentage and the time required. With BDD anodes, complete LVX removal is achieved at all current densities studied in <120 min. Specifically, current densities between 5 and 10 mA cm^{-2} result in complete degradation within 120 min, while increasing the current density to 50 mA cm^{-2} reduces the required time to 60 min. In contrast, complete removal of LVX from hospital effluents using RuO_2/Ti anodes is only possible at current densities of 10 mA cm^{-2} or higher, with complete removal achieved in 60 min. At 5 mA cm^{-2}, the RuO_2/Ti anode attains a removal percentage of 90.7 %, and the experimental data suggests that extending the operating time would likely result in complete LVX removal under these operating conditions.

It is important to point out that LVX degradation at current densities of 10 and 50 mA cm^{-2} is faster with RuO_2/Ti anodes, whereas, at the lower current density (5 mA cm^{-2}), complete removal of the drug is achieved only with BDD anodes. These results underscore the distinct behaviours of each anode material and their influence on the LVX removal process under different operating conditions. For this reason, experimental data were fitted to a first-order kinetics model for comparison purposes, and the resulting kinetic constants (k) are shown in Table 2.

The higher the current density, the higher the kinetic constant for both anodes, consistent with the data shown in Fig. 1. At 5 mA cm^{-2}, the kinetic constant for the BDD anode process is almost twice that of the RuO_2/Ti anode. This difference is attributed to the BDD anode achieving complete LVX removal in 120 min. In contrast, complete pollutant degradation is unattainable within 180 min using the RuO_2/Ti anode, despite the cell potential being quite similar under these operating conditions for both anodes ($V_{BDD} = 5.7$ V; $V_{MMO} = 4.2$ V). As the current

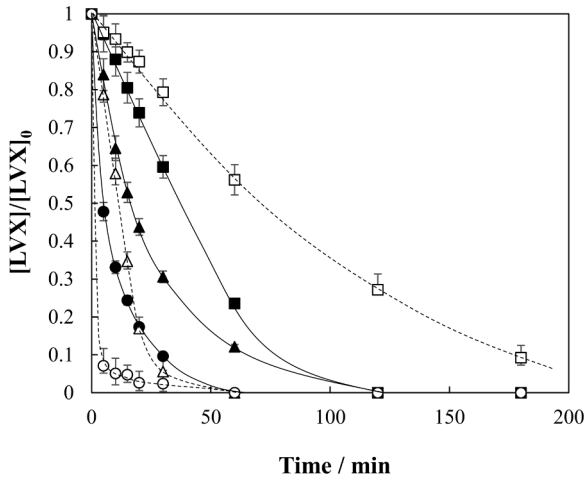

Fig. 1. Influence of the current density on LVX removal during the electrochemical oxidation of synthetic hospital effluents. (■□) 5 mA cm^{-2}; (▲△) 10 mA cm^{-2}; (●○) 50 mA cm^{-2}; $[LVX]_0$: 5 mg dm^{-3}; cathode: SS; T: 25 °C. Black symbols: BDD anode; white symbols: RuO_2/Ti anode.

Table 2
Kinetic constants for the electrolysis of LVX with BDD and RuO_2/Ti anodes.

Anode	j (mA cm^{-2})	k ($0{\cdot}10^{-3}$ min^{-1})	S_R^2 (mg^2 L^{-2})	R^2
BDD	5	24.4 ± 1.81	0.00805	0.96776
	10	35.2 ± 1.36	0.00451	0.99114
	50	74.0 ± 6.83	0.02721	0.95884
RuO_2/Ti	5	12.9 ± 0.60	0.01101	0.98295
	10	99.3 ± 8.27	0.03994	0.96621
	50	102.1 ± 37.81	0.83408	0.55729

density increases, the kinetic constants for RuO_2/Ti anodes become significantly higher, nearly three times those of the BDD anode at 10 mA cm^{-2} and about 25 % higher at 50 mA cm^{-2}. These findings indicate that a current density of 5 mA cm^{-2} is sufficient to remove LVX in <180 min with the BDD anode. In contrast, a minimum current density of 10 mA cm^{-2} is required to achieve complete removal with RuO_2/Ti anode.

The degradation of LVX by electrochemical oxidation can occur via direct oxidation at the anode surface or through mediated oxidation via electrogenerated oxidants and radicals. The dominant mechanism is influenced by the applied current density and the nature of the anode material used [28]. Lower current densities typically favour direct oxidation, whereas higher current densities promote the generation of powerful oxidants and radicals, thus favouring mediated oxidation. The nature of the electrogenerated oxidants and the direct oxidation of the pollutant depend on the electrocatalytic properties of the anode [40]. In this context, the finding that LVX is eliminated at 5 mA cm^{-2} only with BDD anodes, operating at a cell potential comparable to that observed with MMO anodes, suggests that direct oxidation plays a more relevant role under these operating conditions and that BDD anodes are more efficient at this mechanism. The measured cell potentials exceed the chloride oxidation potential to free chlorine (1.4–1.6 V), the predominant species expected to be generated with both anodes given the high chloride content of the effluent. Consequently, low concentrations of these species, evidenced by the LVX degradation results, are generated under these operating conditions. As the current density increases, the cell potential for the BDD anode rises to 6.5 V at 10 mA cm^{-2} and 12.6 V at 50 mA cm^{-2}, whereas MMO anodes exhibit cell potentials of 4.8 V at 10 mA cm^{-2} and 7.9 V at 50 mA cm^{-2}. These results indicate that both direct and indirect oxidation mechanisms can occur during the process at the current densities studied and that the nature and concentration of the oxidants generated can substantially affect LVX degradation kinetics since higher kinetic constants are obtained with MMO anodes at lower cell potentials when applying 10 and 50 mA cm^{-2}. To confirm the contribution of the direct oxidation mechanism at low current densities, the degradation of LVX in 450 mg dm^{-3} $HClO_4$ was investigated using both anodes (Figure S1). This acid concentration was selected to match the conductivity of hospital effluent. $HClO_4$ is an inert medium where LVX degradation occurs primarily via direct pollutant oxidation at the electrode surface or through attack by hydroxyl radicals generated from water oxidation. However, at the current density of 5 mA cm^{-2}, significant generation of hydroxyl radicals is not expected, even with DBB anodes [41], thus making direct oxidation the main degradation mechanism for LVX. The results demonstrate a time-dependent decrease in LVX concentration, albeit at a slightly slower rate compared to that observed in hospital effluent. Nonetheless, the degradation efficiencies achieved (BDD: 100 % and MMO: 79 %) clearly indicate the predominant influence of the direct oxidation mechanism over mediated oxidation under these operating conditions (5 mA cm^{-2}). On the other hand, to assess the role of mediated oxidation in the degradation of LVX, the oxidants electrogenerated during the process with both anodes were monitored, and the results are shown in Fig. 2.

Total oxidants increase with the operating time at all current densities, and the maximum values obtained show a clear positive correlation with the applied current density. Specifically, with BDD anodes, the maximum oxidants reached were 0.57, 0.58 and 0.93 mmol at 5, 10 and

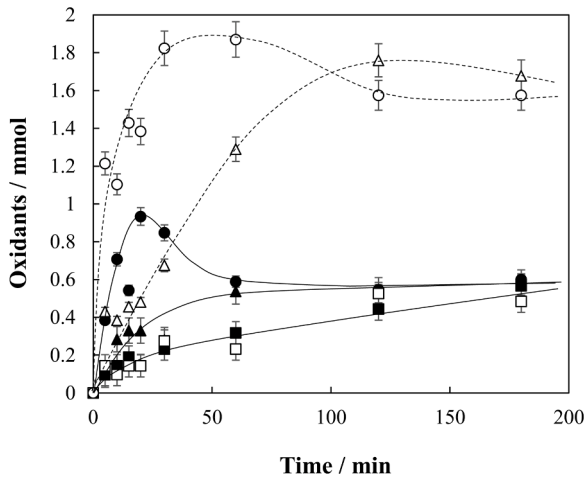

Fig. 2. Influence of the current density on oxidants production during the electrochemical oxidation of synthetic hospital effluents. (■□) 5 mA cm^{-2}; (▲△) 10 mA cm^{-2}; (●○) 50 mA cm^{-2}; $[LVX]_0$: 5 mg dm^{-3}; cathode: SS; T: 25 ºC. Black symbols: BDD anode; white symbols: RuO_2/Ti anode.

50 mA cm^{-2}, respectively, whereas RuO_2/Ti anodes produced 0.53, 1.76 and 1.87 mmol under the same conditions. This behaviour supports the higher LVX removal efficiencies observed at higher current densities (Fig. 1), as a more significant generation of oxidising species accelerates organic pollutant degradation. Furthermore, it reveals the contribution of mediated oxidation to the degradation of LVX in hospital effluents. The oxidant species analysed and shown in Fig. 2 do not represent all the oxidants generated during the process, but only those that have not reacted with the organic matter present in the effluent, which means that higher concentrations could have been produced with both anodes.

A distinct difference between the anode materials is evident. With RuO_2/Ti anodes, during the first hour of reaction, which corresponds to complete LVX degradation, 1.29 and 1.87 mmol of oxidants are generated at 10 and 50 mA cm^{-2}, respectively. In contrast, BDD anodes produce roughly three times fewer oxidants under the same operating conditions (0.54 and 0.59 mmol at 10 and 50 mA cm^{-2}, respectively). This higher generation rate with RuO_2/Ti anodes accounts for the faster degradation observed at higher current densities, as these anodes exhibit a more rapid oxidant generation during the early stages of the reaction compared to BDD.

However, a different behaviour is observed at the lower current density of 5 mA cm^{-2}. Although the overall oxidant production is similar between the two anodes, LVX is removed faster with BDD anodes. This confirms that, at low current densities, direct oxidation at the electrode surface is the dominant mechanism, while mediated oxidation via electrogenerated species plays a lesser role. It is important to note that the nature of the oxidants electrogenerated depends on the electrode material and their interactions with the organic compounds [42,43]. In addition, the different concentrations of electrogenerated oxidants with both anodes largely depend on the nature of the oxidants produced, as they exhibit varying reactivities and, consequently, their stability in the effluent is affected. RuO_2/Ti anodes favour the generation of free chlorine by the electrochemical oxidation of chlorides present in the effluent (Eqs. (1)–3), whereas BDD anodes promote not only the formation of free chlorine species but also the generation of peroxocompounds, such as peroxydisulphate and peroxodiphosphate, by the oxidation of sulphate and phosphate ions (Eqs. (4)–7) [28]. These peroxocompounds possess higher oxidising power than free chlorine, which helps explain why, even at low current densities where both electrodes generate similar amounts of oxidants, the specific oxidant profile produced by BDD anodes results in complete LVX degradation. Nonetheless, the overall quantity of electrogenerated peroxocompounds is expected to be lower than that of free chlorine due to the lower initial concentrations of sulphate or phosphate than chloride ions. Furthermore, free chlorine is more stable than peroxocompounds, so the analysed concentration of the latter, which are mainly generated with BDD anodes, is expected to be lower.

$$2Cl^- \rightarrow Cl_2 + 2e^- \quad (1)$$

$$Cl_2 + H_2O \rightarrow HClO + Cl^- + H^+ \quad (2)$$

$$HClO \rightleftharpoons H^+ + ClO^- \quad (3)$$

$$SO_4^{2-} \rightarrow SO_4^{\cdot-} + e^- \quad (4)$$

$$SO_4^{\cdot-} + SO_4^{\cdot-} \rightarrow S_2O_8^{2-} \quad (5)$$

$$PO_4^{3-} \rightarrow PO_4^{\cdot 2-} + e^- \quad (6)$$

$$PO_4^{\cdot 2-} + PO_4^{\cdot 2-} \rightarrow P_2O_8^{4-} \quad (7)$$

Additionally, both types of electrodes generate hydroxyl radicals from water oxidation (Eq. (8)). However, their interactions with the electrode surfaces differ markedly [44]. RuO_2/Ti anodes chemically interact with hydroxyl radicals, resulting in their adsorption onto the electrode surface. In contrast, BDD anodes promote the physisorption of these radicals, making them more available to react with and degrade organic pollutants. For this reason, RuO_2/Ti anodes are classified as active anodes, while BDD anodes are considered non-active. Furthermore, hydroxyl radicals generated at BDD anodes can react with ions in the effluent, further enhancing the production of oxidising species that contribute to LVX removal (Eqs. (9)–12).

$$H_2O \rightarrow {}^{\cdot}OH + H^+ + e^- \quad (8)$$

$$Cl^- + {}^{\cdot}OH \rightarrow Cl^{\cdot} + OH^- \quad (9)$$

$$Cl^{\cdot} + Cl^{\cdot} \rightarrow Cl_2 \quad (10)$$

$$SO_4^{2-} + {}^{\cdot}OH \rightarrow SO_4^{\cdot-} + OH^- \quad (11)$$

$$PO_4^{3-} + {}^{\cdot}OH \rightarrow PO_4^{\cdot 2-} + OH^- \quad (12)$$

Overall, the oxidants profile suggests that these species are consumed during the degradation of LVX, as indicated by the plateau zone reached at different current densities. This implies that the generation and consumption rates of oxidants become comparable. In some cases, particularly at high current densities, this plateau zone is preceded by a decline in the amount of oxidants in the effluent, which may indicate that the oxidants are being transformed into other species. In this context, the presence of chlorides in the effluent may promote not only the generation of free chlorine but also the generation of more highly oxidised chlorine species, such as chlorate and perchlorate, from electrogenerated hypochlorite oxidation (Equations 13-15). In addition, these chlorine species can also be generated by the reaction of chloride with hydroxyl radicals (Equations 16-19) [31,45].

$$ClO^- + H_2O \rightarrow ClO_2^- + 2H^+ + 2e^- \quad (13)$$

$$ClO_2^- + H_2O \rightarrow ClO_3^- + 2H^+ + 2e^- \quad (14)$$

$$ClO_3^- + H_2O \rightarrow ClO_4^- + 2H^+ + 2e^- \quad (15)$$

$$Cl^- + {}^{\cdot}OH \rightarrow ClO^- + H^+ + e^- \quad (16)$$

$$ClO^- + {}^{\cdot}OH \rightarrow ClO_2^{\cdot-} + H^+ + e^- \quad (17)$$

$$ClO_2^{\cdot-} + {}^{\cdot}OH \rightarrow ClO_3^- + H^+ + e^- \quad (18)$$

$$ClO_3^- + {}^{\cdot}OH \rightarrow ClO_4^{\cdot} + H^+ + e^- \quad (19)$$

Chlorate and perchlorate pose potential risks to human health and the environment by affecting normal metabolism, growth, and development [46]. Consequently, the generation of these species was monitored during the treatment of synthetic hospital effluents polluted with LVX, and the results are plotted in Fig. 3.

As shown in Fig. 3a, chlorate concentration increases with operating time for all current densities studied using the BDD anode. This increase is significantly influenced by current density. Specifically, the maximum chlorate concentrations recorded during the electrochemical oxidation with BDD anodes were 0.75, 3.42 and 2.35 mmol dm^{-3} at 5, 10 and 50 mA cm^{-2}, respectively. Notably, the highest chlorate concentration is not observed at the highest current density, which is likely due to the reactivity of this species.

At current densities below 10 mA cm^{-2}, chlorate concentration increases throughout the experiment. However, at 50 mA cm^{-2}, its concentration exhibits a characteristic profile of a reaction intermediate: an initial increase followed by a decline to a final value below 1 mmol dm^{-3}. This behaviour suggests that chlorate is further oxidised to perchlorate, as evidenced by the significant increase in perchlorate concentration at high current densities, reaching a final maximum value of approximately 7 mmol dm^{-3} (Fig. 3b). In contrast, at 10 mA cm^{-2}, the final perchlorate concentration remains below 0.5 mmol dm^{-3}, which explains the continuously increasing trend in chlorate at this current density. Similarly, at 5 mA cm^{-2}, perchlorate formation is negligible, and chlorate concentration remains low.

On the other hand, electrochemical oxidation with RuO_2/Ti anodes results in maximum chlorate concentrations of 0.23 and 4.29 mmol dm^{-3} at 10 and 50 mA cm^{-2}, respectively, while at lower current densities, chlorate formation is negligible (Fig. 3a). Importantly, no perchlorate formation is detected at any current density when using RuO_2/Ti anodes (Fig. 3b). This is because the electrochemical generation of chlorate and perchlorate primarily occurs by hydroxyl radical-mediated oxidation (Eqs. (18)–19), a process significantly enhanced with BDD anodes due to their electrocatalytic properties as non-active electrodes.

The formation of chlorate and perchlorate during electrochemical oxidation explains the observed decrease in oxidant generation together with the degradation of organics (Fig. 2). Although these species possess a higher oxidation state than free chlorine, they are not reactive under the temperature and pressure conditions of this work. Based on the chlorine speciation results, it is recommended to operate up to 10 mA cm^{-2} when using BDD anodes, as this allows for complete LVX removal within 120 min while minimising chlorate formation in the effluent (no perchlorate concentration was detected under these operating conditions). Likewise, the optimal current density for RuO_2/Ti anodes is 10 mA cm^{-2}, ensuring complete LVX removal in 60 min without the generation of chlorine compounds in a high oxidation state.

In addition to LVX, the synthetic hospital effluents used in this work contain other organic compounds, such as urea and acetate. These compounds are susceptible to oxidation during the process, competing with the degradation of the target pollutant. For this reason, their concentration was monitored over time for all current densities studied with BDD and RuO_2/Ti anodes and results are shown in Fig. 4.

Urea concentration decreases with operating time at all current densities applied for both BDD and RuO_2/Ti anodes (Fig. 4a). Increasing the current density results in higher degradation rates with both anodes, although complete urea removal was achieved only with BDD anodes at 50 mA cm^{-2} within 180 min. At a low current density of 5 mA cm^{-2}, urea removal was 45.76 % with BDD anodes and 30.27 % with RuO_2/Ti anodes. At 10 mA cm^{-2}, both anodes ultimately attained similar final removal percentages. However, the initial degradation rate was higher with BDD anodes. At 50 mA cm^{-2}, RuO_2/Ti anodes achieved a final urea removal of 78.52 %. Overall, these results indicate that BDD anodes provide higher urea removal rates than RuO_2/Ti anodes, likely due to the nature of the electrogenerated oxidants.

On the other hand, acetate concentration decreases over time with BDD anodes, reaching final removal percentages of 25.70, 33.57 and 78.47 % at 5, 10 and 50 mA cm^{-2}, respectively (Fig. 4b). With RuO_2/Ti anodes, significant acetate degradation was observed only at current densities above 10 mA cm^{-2}, with final removal percentages of 24.93 and 27.54 % at 10 and 50 mA cm^{-2}, respectively. These values are lower than those obtained with BDD anodes, which can be attributed to the different electrocatalytic properties of both anodes in generating powerful oxidants and radicals. Interestingly, the initial removal rate of acetate is higher with RuO_2/Ti anodes at 10 and 50 mA cm^{-2}. The higher amount of oxidants electrogenerated with these anodes under these operating conditions may explain this unexpected behaviour. However, these oxidants are transformed from around 60 min onward into chlorine compounds in a high oxidation state (Fig. 3), reducing the effective oxidant pool available for acetate degradation. At 5 mA cm^{-2}, acetate degradation is negligible, and its concentration remains nearly constant in its initial value. These results highlight the refractory nature of acetate compared to urea since its degradation rate is significantly lower despite the initial acetate concentration being nearly half that of urea.

It is important to note that the degradation of urea and acetate is not the primary objective of the treatment process since the focus is selectively degrading the hazardous antibiotic LVX. Urea and acetate do not

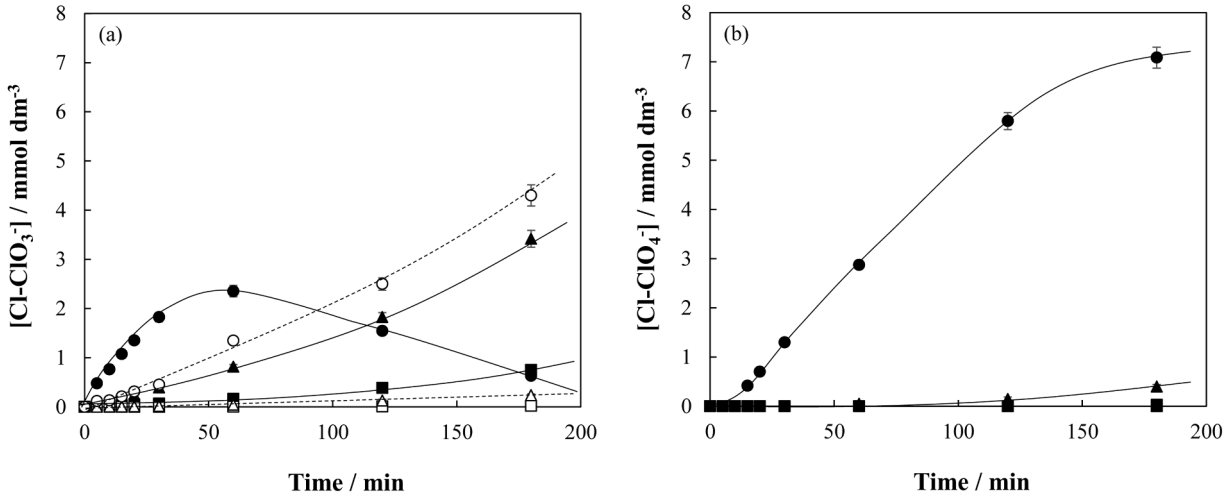

Fig. 3. Influence of the current density on chlorine speciation during the electrochemical oxidation of synthetic hospital effluents. (■□) 5 mA cm^{-2}; (▲△) 10 mA cm^{-2}; (●○) 50 mA cm^{-2}; $[LVX]_0$: 5 mg dm^{-3}; cathode: SS; T: 25 °C. (a) Chlorate; (b) perchlorate; black symbols: BDD anode; white symbols: RuO_2/Ti anode.

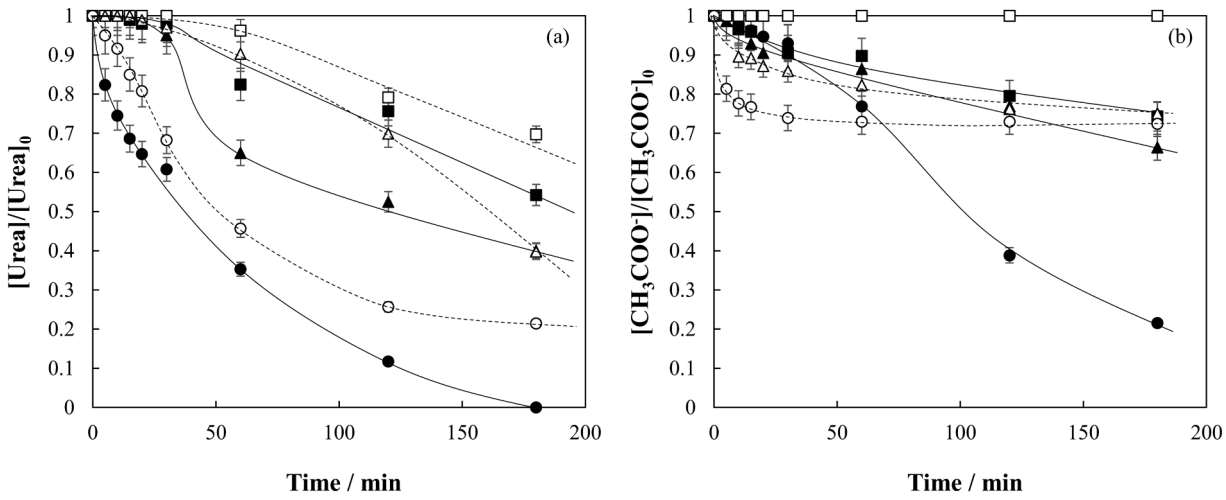

Fig. 4. Influence of the current density on organics removal during the electrochemical oxidation of synthetic hospital effluents. (■□) 5 mA cm^{-2}; (▲Δ) 10 mA cm^{-2}; (●○) 50 mA cm^{-2}; $[LVX]_0$: 5 mg dm^{-3}; cathode: SS; T: 25 °C. (a) Urea; (b) acetate; black symbols: BDD; white symbols: RuO_2/Ti.

pose an environmental risk in the effluent, and their degradation represents a competing reaction that consumes electrons. The superior removal of urea and acetate with BDD anodes at current densities above 10 mA cm^{-2} may partly explain the slightly lower LVX removal rates observed with these anodes than RuO_2/Ti anodes (Fig. 1). Nonetheless, at the operating times required for complete LVX removal with both anodes, the degradation of these organics (urea and acetate) remains lower, indicating that the electrochemical oxidation process selectively targets the antibiotic while only partially degrading other organics present in the effluent. The selective degradation of the target antibiotic can occur through both direct and mediated oxidation mechanisms, with the applied current density playing a crucial role in determining which mechanism predominates, as demonstrated above.

Urea contains two nitrogen atoms, which can be released to the effluent during electrochemical oxidation. Similarly, LVX contains three nitrogen atoms that may also be released during degradation. According to the literature, nitrogen from organic matter is initially oxidised or dissolved in the effluent to nitrite (Eqs. (20)–21) and then rapidly converted to nitrate (Eqs. (22)–23). Additionally, nitrate can be reduced to ammonium at the cathode surface (Eqs. (24)–25) [32]. Synthetic hospital effluents contain low concentrations of nitrate (0.074 mmol dm^{-3}) and ammonium (0.535 mmol dm^{-3}), although these levels can vary due to urea degradation and the subsequent release of nitrogen. Therefore, the evolution of nitrate and ammonium concentrations was monitored, and the results are shown in Fig. 5.

$$N_2 + 2O_2 + 2e^- \rightarrow 2NO_2^- \quad (20)$$

$$N_2 + 4H_2O \rightarrow 2NO_2^- + 8H^+ + 6e^- \quad (21)$$

$$3NO_2^- + 2H^+ \rightleftharpoons 2NO + NO_3^- + H_2O \quad (22)$$

$$NO_2^- + \frac{1}{2}O_2 \rightarrow NO_3^- \quad (23)$$

$$NO_3^- + 6H_2O + 8e^- \rightleftharpoons NH_3 + 9OH^- \quad (24)$$

$$NH_3 + H_2O \rightleftharpoons NH_4^+ + OH^- \quad (25)$$

As can be observed, nitrate concentration increases over time when using both BDD and RuO_2/Ti anodes, regardless of the applied current density (Fig. 5a). This increase indicates that nitrogen from degraded organic compounds is converted into inorganic nitrate during electrochemical oxidation. Furthermore, higher current densities lead to a more significant nitrate generation, which correlates with a more pronounced decrease in LVX (Fig. 1) and urea concentrations (Fig. 4a). Specifically, final nitrate concentrations of 2.665, 4.628 and 8.897

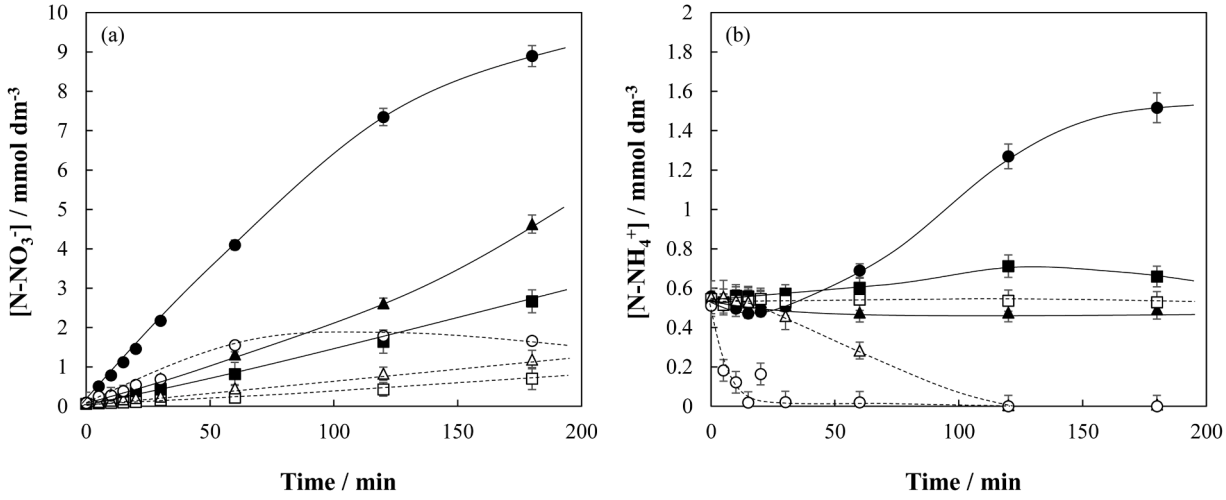

Fig. 5. Influence of the current density on nitrogen speciation during the electrochemical oxidation of synthetic hospital effluents. (■□) 5 mA cm^{-2}; (▲Δ) 10 mA cm^{-2}; (●○) 50 mA cm^{-2}; $[LVX]_0$: 5 mg dm^{-3}; cathode: SS; T: 25 °C. (a) Nitrate; (b) ammonium; black symbols: BDD anode; white symbols: RuO_2/Ti anode.

mmol N dm^{-3} were achieved with BDD anodes at 5, 10 and 50 mA cm^{-2}, respectively, compared to 0.703, 1.184 and 1.660 mmol N dm^{-3} obtained with RuO_2/Ti anodes. As expected, nitrate formation is more pronounced with BDD anodes, which is attributed to the faster urea degradation (the primary nitrogen source in the effluent).

At a low current density (5 mA cm^{-2}), both anodes show a gradual increase in nitrate concentration over time. However, when the current density is increased by 10 (50 mA cm^{-2}), the nitrate generation rate tends to decrease or stabilise at the end of the process, suggesting that nitrate is reduced to ammonium under these operating conditions. This hypothesis is supported by the evolution of ammonium concentration depicted in Fig. 5b With BDD anodes at 50 mA cm^{-2}, ammonium concentration increases significantly, reaching a final value of 1.517 mmol N dm^{-3}. In contrast, at current densities lower than 10 mA cm^{-2}, ammonium levels remain nearly constant, indicating that nitrate reduction is not favoured at these operating conditions.

A markedly different behaviour is observed with RuO_2/Ti anodes. At 5 mA cm^{-2}, the ammonium concentration remains nearly constant, while at 10 and 50 mA cm^{-2}, it decreases over time until it is eliminated after 120 min. The nature of the oxidants generated likely influences this behaviour. RuO_2/Ti anodes enhance the electrochemical generation of free chlorine from chloride oxidation (Fig. 2). The resulting hypochlorite, produced in significant concentrations at higher current densities, can react with ammonium to form inorganic chloramines (Eqs. (26)–28) [47].

$$NH_4^+ + ClO^- \rightarrow NH_2Cl + H_2O \quad (26)$$

$$NH_2Cl + HClO \rightarrow NHCl_2 + H_2O \quad (27)$$

$$NHCl_2 + HClO \rightarrow NCl_3 + H_2O \quad (28)$$

Consequently, the observed decrease in ammonium concentration with RuO_2/Ti anodes at 10 and 50 mA cm^{-2} is likely due to chloramine formation. These combined chlorine species contribute to LVX degradation, but their oxidising power is lower than that of free chlorine. Although synthetic hospital effluent initially contains only low concentrations of nitrate and ammonium, these species should not increase significantly during the treatment, as elevated nitrate levels can pose health and environmental risks. Under moderate operating conditions, the complete removal of LVX with BDD anodes at 5 mA cm^{-2} results in a maximum nitrate concentration of 1.641 mmol N dm^{-3}. In contrast, the ammonium concentration remains at its initial value of 0.535 mmol N dm^{-3}. Similarly, when LVX is wholly removed using RuO_2/Ti anodes at 10 mA cm^{-2}, the final nitrate concentration is only 0.456 mmol N dm^{-3}, and the ammonium concentration decreases to 0.283 mmol N dm^{-3}.

The degradation of LVX and other organics (urea and acetate) by electrochemical oxidation can lead to the complete mineralisation of the organic matter or the formation of other intermediate organic compounds. Total Organic Carbon (TOC) was analysed during the electrochemical oxidation at different current densities with BDD and RuO_2/Ti anodes to evaluate the mineralisation grade. Fig. 6 shows the TOC evolution as a function of the operating time when treating synthetic hospital effluents polluted with LVX.

TOC decreases with the operation time for all current densities tested with both anodes. However, complete mineralisation of the organic matter in the effluent is not achieved, regardless of the current density and anode material used. This is an expected behaviour because only LVX is completely removed (Fig. 1), while urea and acetate are only partially degraded (Fig. 4), accumulating significant intermediate compounds. With RuO_2/Ti anodes, the mineralisation percentage increases slightly with the current density, with TOC removal reaching 10.09, 32.83 and 54.11 % at 5, 10 and 50 mA cm^{-2}, respectively. A similar trend is observed with BDD anodes, which achieve maximum mineralisation percentages of 41.55, 45.19 and 83.80 % at 5, 10 and 50 mA cm^{-2}, respectively.

These results confirm that BDD anodes facilitate the degradation of

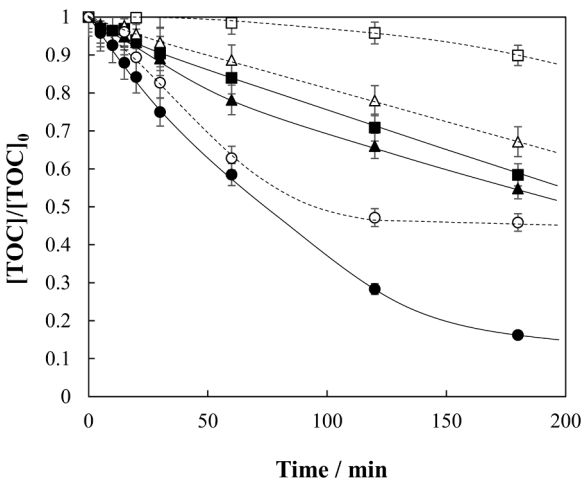

Fig. 6. Influence of the current density on TOC removal during the electrochemical oxidation of synthetic hospital effluents. (■□) 5 mA cm^{-2}; (▲△) 10 mA cm^{-2}; (●○) 50 mA cm^{-2}; $[TOC]_0$: 149.77 mg dm^{-3}; $[LVX]_0$: 5 mg dm^{-3}; cathode: SS; T: 25 °C. black symbols: BDD anode; white symbols: RuO_2/Ti anode.

the target antibiotic and enhance the mineralisation of the organic matter to a greater extent. In contrast, the decreasing trend observed during electrochemical oxidation with RuO_2/Ti anodes suggests that similar mineralisation levels might be achieved if the operating time were increased. Overall, the experimental data reflect the distinct electrocatalytic behaviours of both electrodes. BDD anodes, characterised by a higher overpotential for oxygen evolution, favour the production of hydroxyl radicals and thus promote the electrochemical combustion of the organic matter in the effluent. Meanwhile, RuO_2/Ti anodes typically follow an electrochemical conversion pathway, transforming organics into partially oxidised intermediates over shorter operation times. This difference helps explain the higher mineralisation rates with BDD anodes, particularly at higher current densities [48].

To gain insight into the degradation of LVX from hospital effluents by electrochemical oxidation with both anodes, the organic intermediates formed were analysed by HPLC-MS coupled with a QTOF mass detector. For this purpose, experiments conducted at 10 mA cm^{-2} with BDD and RuO_2/Ti anodes were selected to compare the compounds generated under similar operating conditions. This current density was chosen because it is the lowest value at which LVX is fully degraded with both anodes. The analysed samples were selected at key points during the reaction: one sample at the beginning of the process, another when 50 % of the antibiotic had been degraded, and a final sample when the antibiotic had been completely removed from the effluent. Table 3 summarises the main intermediates identified during the electrochemical oxidation of synthetic hospital effluents polluted with LVX using BDD and RuO_2/Ti anodes. The technique used has limitations for determining the exact positions of functional groups without additional fragmentation studies or NMR analysis. However, the most likely hydroxylation positions can be proposed based on typical degradation pathways reported in the literature and supported by the observed mass shifts [49–51].

HPLC-MS analysis revealed that 13 main intermediate organic compounds were formed during the electrochemical oxidation of synthetic hospital effluents polluted with LVX using BDD and RuO_2/Ti anodes. More of these intermediates were detected with RuO_2/Ti anodes (12) than with BDD anodes (6). Since some of these LVX degradation by-products may be even more hazardous than the parent pollutant, a toxicity analysis was conducted using the ECOSAR software. Based on their quantitative structure, this tool evaluates the potential aquatic ecotoxicity (both acute and chronic) of chemicals toward various marine organisms, including fish, *Daphnia* and green algae. In this study, the

Table 3
Main intermediates formed during the degradation of LVX from synthetic hospital effluents by electrochemical oxidation at 10 mA cm^{-2}.

No.	*m/z* (elemental composition predicted)	*m/z* (elemental composition experimental)	T_R (min)	Molecular formula	Proposed molecular structure	Anode
P1	377.1387	377.1451	3.02	$C_{18}H_{20}FN_3O_5$	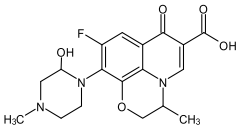	BDD RuO_2/ Ti
P2	351.1230	351.1219	2.05	$C_{16}H_{18}FN_3O_5$	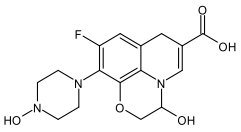	BDD RuO_2/ Ti
P3	347.1281	347.1147	3.00	$C_{17}H_{18}FN_3O_4$	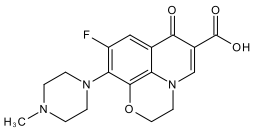	RuO_2/ Ti
P4	335.1281	335.1352	3.20	$C_{16}H_{18}FN_3O_4$	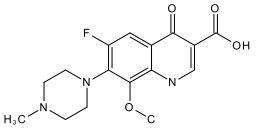	RuO_2/ Ti
P5	307.0968	307.0722	3.80	$C_{14}H_{14}FN_3O_4$	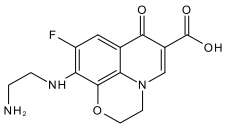	RuO_2/ Ti
P6	305.1176	305.093	5.10	$C_{15}H_{16}FN_3O_3$	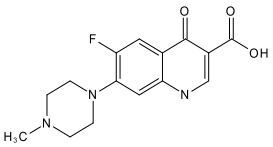	RuO_2/ Ti
P7	305.1176	305.0679	6.10	$C_{15}H_{16}FN_3O_3$	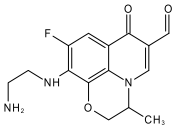	RuO_2/ Ti
P8	295.0957	295.2576	8.04	$C_{16}H_{13}N_3O_3$	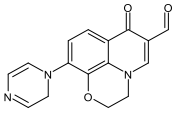	BDD
P9	280.0859	279.2625	8.01	$C_{13}H_{13}FN_2O_4$	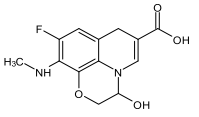	BDD RuO_2/ Ti
P10	278.0703	278.0775	4.40	$C_{13}H_{11}FN_2O_4$	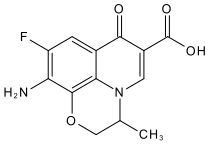	RuO_2/ Ti
P11	274.0954	274.2732	6.04	$C_{14}H_{14}N_2O_4$	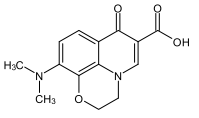	BDD RuO_2/ Ti
P12	269.1164	269.3146	3.05	$C_{15}H_{15}N_3O_2$	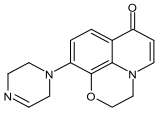	BDD RuO_2/ Ti

(*continued on next page*)

Table 3 (*continued*)

No.	*m/z* (elemental composition predicted)	*m/z* (elemental composition experimental)	T_R (min)	Molecular formula	Proposed molecular structure	Anode
P13	263.1434	263.0666	5.50	$C_{14}H_{18}FN_3O$	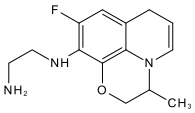	RuO_2/Ti

acute and chronic toxicities of the degradation by-products were assessed for these three organisms. The results are presented in Table 4, with colour coding according to the GHS system (Globally Harmonized System of Classification and Labeling of Chemicals): green for non-toxic effects (> 100 mg dm^{-3}), yellow for harmful effects (10–100 mg dm^{-3}), orange for toxic effects (1–10 mg dm^{-3}), and red for very toxic effects (< 1 mg dm^{-3}) [52]. The identified functional groups in these intermediates include primarily aliphatic amines (AA), neutral organics (NO), vinyl/ allyl/ propargyl ketones (V/A/PK), vinyl/ allyl/ propargyl aldehydes (V/A/PA) and anilines (A).

As can be observed, 7 LVX by-products (P1, P3, P4, P5, P6, P9 and P11) are considered non-toxic to the evaluated species because they lack functional groups associated with harmful effects. Of these, 5 were generated exclusively with the RuO_2/Ti anode and 2 were produced with both electrodes. In contrast, only 1 of the 13 identified intermediates (P12) exhibits toxicity across all the species studied with both anodes. This finding suggests that under the operating conditions tested, the electrocatalytic properties of RuO_2/Ti anodes favour the formation of more toxic species.

For the remaining intermediates, toxicity varies depending on the species and the functional groups present. For instance, P2 exhibits chronic toxicity only to *Daphnia* in the AA group, while P10 stands out for its toxicity in the A group. However, it is important to note that these toxic intermediates are present at much lower concentrations than the parent compound, reducing their overall environmental impact.

These results reveal that at 10 mA cm^{-2}, RuO_2/Ti anodes generate more toxic intermediate compounds than BDD anodes. However, the hazard associated with these compounds could be substantially reduced if the operating time were extended to achieve complete mineralisation of the organic matter, although this would increase the energy requirements of the process.

Based on the intermediates identified and the toxicity analysis, different LVX degradation pathways have been proposed for RuO_2/Ti anodes since this electrode promotes the formation of more intermediate compounds. A sequence of reactions involving de-piperazinyl, de-methylation, decarboxylation, dehydration, defluorination, and quinolone ring opening can be achieved during the electrochemical oxidation of synthetic hospital effluents polluted with LVX. Fig. 7 shows the proposed degradation pathways.

The first pathway involves the formation of P2 (*m/z* = 351.33) via the substitution of a methyl group by a hydroxyl group. Subsequently, P2 undergoes de-methylation and de-piperazinyl to yield P9 (*m/z* =

Table 4
Estimated toxicities for the main LVX degradation by-products identified using the ECOSAR program. (■) Non-toxic (>100 mg dm^{-3}), (■) harmful (10–100 mg dm^{-3}), (■) toxic (1–10 mg dm^{-3}), (■) very toxic (<1 mg dm^{-3}).

Compounds	Classes of ECOSAR	Acute toxicity (mg dm^{-3})			Chronic toxicity (mg dm^{-3})			Anode
		Fish (LC_{50}-96h)	*Daphnia* (LC_{50}-48h)	Algae (EC_{50}-96h)	Fish (CV)	*Daphnia* (CV)	Algae (CV)	
P1	AA	$2.7{\cdot}10^5$	$1.6{\cdot}10^4$	$3.12{\cdot}10^4$	$4.54{\cdot}10^4$	861	$7.56{\cdot}10^3$	BDD RuO_2/Ti
	NO	$7.06{\cdot}10^6$	$2.84{\cdot}10^6$	$5.07{\cdot}10^5$	$1.06{\cdot}10^5$	$6.16{\cdot}10^4$	$9.62{\cdot}10^4$	
	V/A/PK	$1.57{\cdot}10^5$	$1.1{\cdot}10^5$	$9.22{\cdot}10^5$	$4.51{\cdot}10^6$	$1.86{\cdot}10^4$	$7.7{\cdot}10^4$	
P2	AA	$1.1{\cdot}10^4$	$1.32{\cdot}10^3$	$1.73{\cdot}10^3$	$1.66{\cdot}10^3$	86.6	486	BDD RuO_2/Ti
	NO	$1.82{\cdot}10^5$	$8.6{\cdot}10^4$	$2.98{\cdot}10^4$	$1.43{\cdot}10^4$	5.10^3	$5.17{\cdot}10^3$	
P3	AA	$3.5{\cdot}10^4$	$3.08{\cdot}10^3$	$4.63{\cdot}10^3$	$5.15{\cdot}10^3$	188	$1.2{\cdot}10^3$	RuO_2/Ti
	NO	$6.4{\cdot}10^5$	$2.85{\cdot}10^5$	$7.82{\cdot}10^4$	$4.7{\cdot}10^4$	$1.42{\cdot}10^4$	$1.2{\cdot}10^4$	
	V/A/PK	$3.67{\cdot}10^4$	$2.54{\cdot}10^4$	$1.41{\cdot}10^5$	$3.55{\cdot}10^5$	$3.05{\cdot}10^3$	$2.07{\cdot}10^3$	
P4	AA	$6.52{\cdot}10^4$	$5.45{\cdot}10^3$	$9.08{\cdot}10^3$	$1.12{\cdot}10^4$	317	$2.33{\cdot}10^3$	RuO_2/Ti
	NO	$1.52{\cdot}10^6$	$6.5{\cdot}10^5$	$1.51{\cdot}10^5$	$1.06{\cdot}10^5$	$2.89{\cdot}10^4$	$2.11{\cdot}10^4$	
	V/A/PK	$6.03.10^4$	$4.2.10^4$	$2.7.10^5$	$8.9{\cdot}10^5$	$5.76{\cdot}10^3$	$3.23{\cdot}10^3$	
P5	AA	$1.66{\cdot}10^5$	$1.29{\cdot}10^4$	$2.5{\cdot}10^4$	$3.63{\cdot}10^4$	693	$6.08{\cdot}10^3$	RuO_2/Ti
	NO	$5.64.10^6$	$2.27.10^6$	$4.07.10^5$	$3.67.10^5$	$8.49.10^4$	$4.95.10^4$	
	V/A/PK	$1.27{\cdot}10^5$	$8.96{\cdot}10^4$	$7.41{\cdot}10^5$	$3.6{\cdot}10^6$	$1.5{\cdot}10^4$	$6.21{\cdot}10^3$	
P6	AA	$6.71{\cdot}10^4$	$5.56{\cdot}10^3$	$9.43{\cdot}10^3$	$1.19{\cdot}10^4$	330	$2.41{\cdot}10^3$	RuO_2/Ti
	NO	$1.63{\cdot}10^6$	$6.95{\cdot}10^5$	$1.56{\cdot}10^5$	$1.14{\cdot}10^5$	$3.03{\cdot}10^4$	$2.15{\cdot}10^4$	
	V/A/PK	$6.06{\cdot}10^4$	$4.24{\cdot}10^4$	$2.83{\cdot}10^5$	$9.67{\cdot}10^5$	$5.9{\cdot}10^3$	$3.21{\cdot}10^3$	
P7	AA	985	94.5	120	111	6.29	34	RuO_2/Ti
	NO	$1.19{\cdot}10^4$	$5.67{\cdot}10^3$	$2.07{\cdot}10^3$	946	342	370	
	V/A/PK	$1.28{\cdot}10^3$	876	$3.69{\cdot}10^3$	$5.98{\cdot}10^3$	84.2	79.9	
P8	NO	592	323	204	55.2	28.2	48.9	BDD
	V/A/PK	214	143	358	249	8.95	16	
	V/A/PA	1.01	2.06	0.386	0.067	0.045	0.101	
P9	NO	$5.64{\cdot}10^4$	$2.78{\cdot}10^4$	$1.15{\cdot}10^4$	$4.66{\cdot}10^3$	$1.82{\cdot}10^3$	$2.18{\cdot}10^3$	RuO_2/Ti
P10	A	$1.77{\cdot}10^3$	57.9	185	28.8	0.634	82.3	RuO_2/Ti
	NO	$2.62{\cdot}10^4$	$1.33{\cdot}10^4$	$6.33{\cdot}10^3$	$2.25{\cdot}10^3$	960	$1.30{\cdot}10^3$	
	V/A/PK	$5.04{\cdot}10^3$	$3.41{\cdot}10^3$	$1.12{\cdot}10^4$	$1.21{\cdot}10^4$	267	343	
P11	NO	$9.63{\cdot}10^3$	$5.13{\cdot}10^3$	$2.29{\cdot}10^3$	872	417	662	BDD RuO_2/Ti
	V/A/PK	$2.77{\cdot}10^3$	$1.86{\cdot}10^3$	$5.13{\cdot}10^3$	$4.20{\cdot}10^3$	126	201	
P12	NO	49.3	29.9	29.4	5.22	3.52	8.94	BDD RuO_2/Ti
	V/A/PK	-	30.9	50.9	18.0	1.37	4.11	
P13	AA	42.3	5.11	4.10	2.36	0.425	1.38	RuO_2/Ti
	NO	169	97.2	75.7	16.8	9.77	20.3	

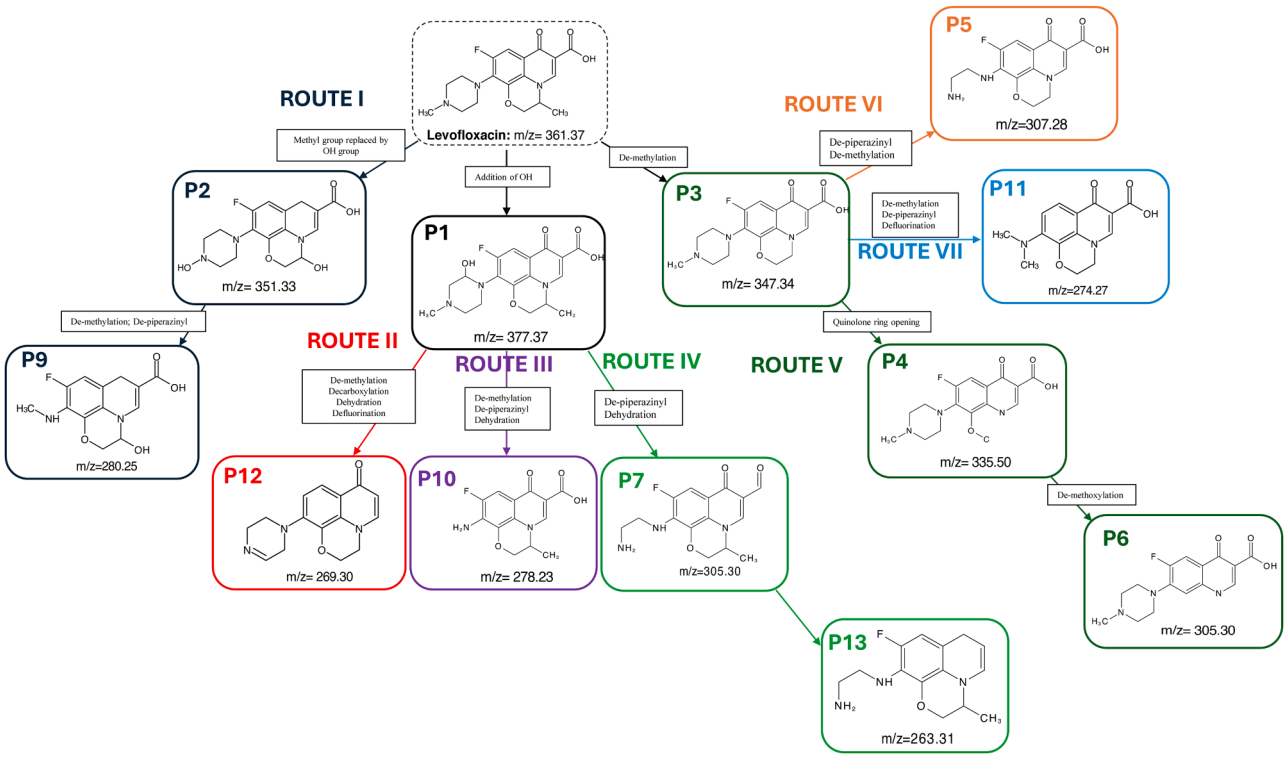

Fig. 7. LVX degradation pathways proposed for the electrochemical oxidation of synthetic hospital effluents with RuO_2/Ti anode at 10 mA cm^{-2}.

280.25). In the second pathway, the addition of a hydroxyl group leads to the formation of P1 (m/z = 377.37), which then undergoes de-methylation, decarboxylation, dehydration, and defluorination to form P12 (m/z = 269.30). Alternatively, via a third route, P1 can be degraded through de-methylation, de-piperazinyl, and dehydration to produce P10 (m/z = 278.23). The fourth pathway results in the formation of P7 (m/z = 305.30) through de-piperazinyl and dehydration.

In the fifth pathway, de-methylation leads to the formation of P3 (m/z = 347.34). This intermediate then undergoes further modifications, including quinolone ring opening and de-methoxylation, resulting in different degradation products: P4 (m/z = 335.50) and P6 (m/z = 305.30), respectively. The sixth pathway involves the transformation of P3 via piperazine ring opening and de-methylation to form P5 (m/z = 307.28). Finally, the seventh pathway forms P11 (m/z = 274.27) through de-methylation, de-piperazinyl, and defluorination.

Based on these proposed pathways and previous literature [53–55], it can be assumed that the next stage in the degradation process involves further oxidation into low molecular weight carboxylic acids, ultimately leading to the complete mineralisation of the organic matter to CO_2 and H_2O.

4. Conclusions

This study demonstrates that electrochemical oxidation is highly effective for treating synthetic hospital effluents contaminated with 5 mg dm^{-3} of levofloxacin (LVX). The following conclusions can be drawn from this work:

- Using BDD anodes, complete degradation of LVX was achieved across a wide range of current densities (5 - 50 mA cm^{-2}), with higher currents significantly enhancing the degradation rate due to the increased production of oxidising species. Although MMO anodes (such as RuO_2/Ti) yielded slightly faster LVX oxidation rates at higher currents, the overall process efficiency was strongly influenced by the nature and amount of electrogenerated oxidants.
- The study revealed distinct chlorine speciation depending on the anode material: BDD anodes generated chlorates and perchlorates, whereas only chlorates were detected with RuO_2/Ti anodes. Notably, the concentration of these chlorine species remained negligible during the period required for complete LVX removal.
- The electrochemical oxidation process targeted LVX and facilitated the degradation of other organic constituents, such as urea and acetate, in the synthetic effluent. However, the treatment exhibited selectivity toward LVX, which was degraded more rapidly than these competing organics.
- The oxidation of urea resulted in the release of nitrogen, which was subsequently transformed into nitrite, nitrate, and ultimately ammonium. When using RuO_2/Ti anodes, the ammonium reacted with free chlorine to form chloramines, contributing further to the disinfection process.
- A comparative analysis between active (RuO_2/Ti) and non-active (BDD) anodes revealed that while RuO_2/Ti anodes favour electrochemical conversion pathways, BDD anodes promote electrochemical combustion. This is evidenced by the higher Total Organic Carbon (TOC) removal (exceeding 80 % across the tested current densities) achieved with BDD anodes.
- Finally, the identification of LVX degradation intermediates via HPLC-MS enabled the proposal of several mineralisation pathways, which include piperazine ring opening, de-piperazinylation, de-methylation, and decarboxylation. The experiments detected more intermediates using RuO_2/Ti anodes, indicating more complex degradation mechanisms.

Declaration of competing interest

The authors declare that they have no known competing financial interests or personal relationships that could have appeared to influence the work reported in this paper.

Acknowledgements

This research is part of the project TEC-2024/ECO-69 (CARESOIL-CM) funded by the Community of Madrid, the network RED2022-134552-T (E3TECH+) funded by MICIU/AEI/10.13039/501100011 and the grant CNS2022–135764 funded by MICIU/AEI/10.13039/501100011033 and by European Union NextGenerationEU/PRTR. J.L.S. Duarte also acknowledges the funding received through the grant 2023-T1/ECO-29390 from the "Atracción de Talento César Nombela" program of the Community of Madrid.

Supplementary materials

Supplementary material associated with this article can be found, in the online version, at doi:10.1016/j.electacta.2025.146390.

References

[1] M. Priyadarshini, A. Ahmad, S. Das, M.M. Ghangrekar, Application of innovative electrochemical and microbial electrochemical technologies for the efficacious removal of emerging contaminants from wastewater: a review, J. Environ. Chem. Eng. (2022) 108230.
[2] E.M. Sunderland, X.C. Hu, C. Dassuncao, A.K. Tokranov, C.C. Wagner, J.G. Allen, A review of the pathways of human exposure to poly- and perfluoroalkyl substances (PFASs) and present understanding of health effects, J. Expos. Sci. Env. Epidemiol 29 (2019) 131–147.
[3] H. Ali, E. Khan, I. Ilahi, Environmental chemistry and ecotoxicology of hazardous heavy metals: environmental persistence, toxicity, and bioaccumulation, J. Chem. 2019 (2019).
[4] M. Tudi, H.D. Ruan, L. Wang, J. Lyu, R. Sadler, D. Connell, C. Chu, D.T. Phung, Agriculture development, pesticide application and its impact on the environment, Int. J. Env. Res. Public Health 18 (2021) 1–24.
[5] J. Fick, H. Söderström, R.H. Lindberg, C. Phan, M. Tysklind, D.J. Larsson, Contamination of surface, ground, and drinking water from pharmaceutical production, Environ. Toxicol. Chem. 28 (2009) 2522–2527.
[6] S. Fekadu, E. Alemayehu, R. Dewil, B. Van der Bruggen, Pharmaceuticals in freshwater aquatic environments: a comparison of the African and European challenge, Sci. Total. Environ. 654 (2019) 324–337.
[7] E. Emmanuel, Y. Perrodin, G. Keck, J.-M. Blanchard, P. Vermande, Ecotoxicological risk assessment of hospital wastewater: a proposed framework for raw effluents discharging into urban sewer network, J. Hazard. Mater. 117 (2005) 1–11.
[8] S.K. Behera, H.W. Kim, J.-E. Oh, H.-S. Park, Occurrence and removal of antibiotics, hormones and several other pharmaceuticals in wastewater treatment plants of the largest industrial city of Korea, Sci. Total. Environ. 409 (2011) 4351–4360.
[9] A. Ginebreda, I. Muñoz, M.L. de Alda, R. Brix, J. López-Doval, D. Barceló, Environmental risk assessment of pharmaceuticals in rivers: relationships between hazard indexes and aquatic macroinvertebrate diversity indexes in the Llobregat River (NE Spain), Env. Int 36 (2010) 153–162.
[10] A. Jelic, M. Gros, A. Ginebreda, R. Cespedes-Sánchez, F. Ventura, M. Petrovic, D. Barcelo, Occurrence, partition and removal of pharmaceuticals in sewage water and sludge during wastewater treatment, Water. Res. 45 (2011) 1165–1176.
[11] N. Le-Minh, S.J. Khan, J.E. Drewes, R.M. Stuetz, Fate of antibiotics during municipal water recycling treatment processes, Water. Res. 44 (2010) 4295–4323.
[12] W.H. Organization, Global Health Estimates: life expectancy and leading causes of death and disability, World Health Organ. (2019).
[13] C.-A.J. FMFRA, Actualizacion en la prescripción de fluoroquinolonas, Med. Interna Mex. (2018) 89–105.
[14] C.J.L. Murray, K.S. Ikuta, F. Sharara, L. Swetschinski, G.Robles Aguilar, A. Gray, C. Han, C. Bisignano, P. Rao, E. Wool, S.C. Johnson, A.J. Browne, M.G. Chipeta, F. Fell, S. Hackett, G. Haines-Woodhouse, B.H. Kashef Hamadani, E.A.P. Kumaran, B. McManigal, S. Achalapong, R. Agarwal, S. Akech, S. Albertson, J. Amuasi, J. Andrews, A. Aravkin, E. Ashley, F.-X. Babin, F. Bailey, S. Baker, B. Basnyat, A. Bekker, R. Bender, J.A. Berkley, A. Bethou, J. Bielicki, S. Boonkasidecha, J. Bukosia, C. Carvalheiro, C. Castañeda-Orjuela, V. Chansamouth, S. Chaurasia, S. Chiurchiù, F. Chowdhury, R. Clotaire Donatien, A.J. Cook, B. Cooper, T. R. Cressey, E. Criollo-Mora, M. Cunningham, S. Darboe, N.P.J. Day, M. De Luca, K. Dokova, A. Dramowski, S.J. Dunachie, T. Duong Bich, T. Eckmanns, D. Eibach, A. Emami, N. Feasey, N. Fisher-Pearson, K. Forrest, C. Garcia, D. Garrett, P. Gastmeier, A.Z. Giref, R.C. Greer, V. Gupta, S. Haller, A. Haselbeck, S.I. Hay, M. Holm, S. Hopkins, Y. Hsia, K.C. Iregbu, J. Jacobs, D. Jarovsky, F. Javanmardi, A. W.J. Jenney, M. Khorana, S. Khusuwan, N. Kissoon, E. Kobeissi, T. Kostyanev, F. Krapp, R. Krumkamp, A. Kumar, H.H. Kyu, C. Lim, K. Lim, D. Limmathurotsakul, M.J. Loftus, M. Lunn, J. Ma, A. Manoharan, F. Marks, J. May, M. Mayxay, N. Mturi, T. Munera-Huertas, P. Musicha, L.A. Musila, M.M. Mussi-Pinhata, R.N. Naidu, T. Nakamura, R. Nanavati, S. Nangia, P. Newton, C. Ngoun, A. Novotney, D. Nwakanma, C.W. Obiero, T.J. Ochoa, A. Olivas-Martinez, P. Olliaro, E. Ooko, E. Ortiz-Brizuela, P. Ounchanum, G.D. Pak, J.L. Paredes, A.Y. Peleg, C. Perrone, T. Phe, K. Phommasone, N. Plakkal, A. Ponce-de-Leon, M. Raad, T. Ramdin, S. Rattanavong, A. Riddell, T. Roberts, J.V. Robotham, A. Roca, V.D. Rosenthal, K. E. Rudd, N. Russell, H.S. Sader, W. Saengchan, J. Schnall, J.A.G. Scott, S. Seekaew, M. Sharland, M. Shivamallappa, J. Sifuentes-Osornio, A.J. Simpson, N. Steenkeste, A.J. Stewardson, T. Stoeva, N. Tasak, A. Thaiprakong, G. Thwaites, C. Tigoi, C. Turner, P. Turner, H.R. van Doorn, S. Velaphi, A. Vongpradith, M. Vongsouvath, H. Vu, T. Walsh, J.L. Walson, S. Waner, T. Wangrangsimakul, P. Wannapinij, T. Wozniak, T.E.M.W. Young Sharma, K.C. Yu, P. Zheng, B. Sartorius, A.D. Lopez, A. Stergachis, C. Moore, C. Dolecek, M. Naghavi, Global burden of bacterial antimicrobial resistance in 2019: a systematic analysis, Lancet 399 (2022) 629–655.
[15] R. Davis, H.M. Bryson, Levofloxacin: a review of its antibacterial activity, Pharmacokinet. Ther. Effic. Drugs 47 (1994) 677–700.
[16] H. Wei, D. Hu, J. Su, K. Li, Intensification of levofloxacin sono-degradation in a US/H2O2 system with Fe3O4 magnetic nanoparticles, Chin. J. Chem. Eng. 23 (2015) 296–302.
[17] R. Al Abri, F. Al Marzouqi, A.T. Kuvarega, M.A. Meetani, S.M.Z. Al Kindy, S. Karthikeyan, Y. Kim, R. Selvaraj, Nanostructured cerium-doped ZnO for photocatalytic degradation of pharmaceuticals in aqueous solution, J. Photochem. Photobiol. A: Chem. 384 (2019) 112065.
[18] Á. Moratalla, S. Cotillas, E. Lacasa, C.M. Fernández-Marchante, S. Ruiz, A. Valladolid, P. Cañizares, M.A. Rodrigo, C. Sáez, Occurrence and toxicity impact of pharmaceuticals in hospital effluents: simulation based on a case of study, Process Saf. Env.. Prot 168 (2022) 10–21.
[19] C.M. El-Maraghy, O.M. El-Borady, O.A. El-Naem, Effective removal of levofloxacin from pharmaceutical wastewater using synthesized zinc oxid, graphen oxid nanoparticles compared with their combination, Sci. Rep. 10 (2020) 5914.
[20] B.L. Phoon, C.C. Ong, M.S. Mohamed Saheed, P.L. Show, J.S. Chang, T.C. Ling, S. S. Lam, J.C. Juan, Conventional and emerging technologies for removal of antibiotics from wastewater, J. Hazard. Mater. (2020) 400.
[21] D. Nasuhoglu, A. Rodayan, D. Berk, V. Yargeau, Removal of the antibiotic levofloxacin (LEVO) in water by ozonation and TiO_2 photocatalysis, Chem. Eng. J. 189 (2012) 41–48.
[22] L.A. Goulart, A. Moratalla, P. Cañizares, M.R.V. Lanza, C. Sáez, M.A. Rodrigo, High levofloxacin removal in the treatment of synthetic human urine using Ti/MMO/ZnO photo-electrocatalyst, J. Environ. Chem. Eng. (2022) 10.
[23] N. Barhoumi, L. Labiadh, M.A. Oturan, N. Oturan, A. Gadri, S. Ammar, E. Brillas, Electrochemical mineralization of the antibiotic levofloxacin by electro-fenton-pyrite process, Chemosphere 141 (2015) 250–257.
[24] X. Xue, W. Liao, D. Liu, X. Zhang, Y. Huang, MgO/Co_3O_4 composite activated peroxymonosulfate for levofloxacin degradation: role of surface hydroxyl and oxygen vacancies, Sep. Purif. Technol. 306 (2023) 122560.
[25] X. Jia, C. Wang, X. Zhao, Y. Li, H. He, J. Wu, Y. Yang, Levofloxacin degradation in electro-fenton system with FeMn@GF composite electrode, J. Environ. Chem. Eng. 12 (2024) 114625.
[26] J.F. Carneiro, J.M. Aquino, B.F. Silva, A.J. Silva, R.C. Rocha-Filho, Comparing the electrochemical degradation of the fluoroquinolone antibiotics norfloxacin and ciprofloxacin using distinct electrolytes and a BDD anode: evolution of main oxidation byproducts and toxicity, J. Environ. Chem. Eng. 8 (2020) 104433.
[27] L. Zhu, B. Santiago-Schübel, H. Xiao, H. Hollert, S. Kueppers, Electrochemical oxidation of fluoroquinolone antibiotics: mechanism, residual antibacterial activity and toxicity change, Water. Res. 102 (2016) 52–62.
[28] S. Cotillas, E. Lacasa, M. Herraiz, C. Sáez, P. Cañizares, M.A. Rodrigo, The role of the anode material in selective penicillin G oxidation in urine, ChemElectroChem. 6 (2019) 1376–1384.
[29] Q. Yuan, S. Qu, R. Li, Z.Y. Huo, Y. Gao, Y. Luo, Degradation of antibiotics by electrochemical advanced oxidation processes (EAOPs): performance, mechanisms, and perspectives, Sci. Total. Environ. 856 (2023).
[30] M. Voigt, M. Jaeger, Chapter 36 - In silico and in vivo ecotoxicity—QSAR-based predictions and experimental assays for the aquatic environment (Ed.), in: H. Hong (Ed.), QSAR in Safety Evaluation and Risk Assessment, Academic Press, 2023, pp. 495–509.
[31] M. Herraiz-Carboné, A. Santos, A. Checa-Fernández, C.M. Domínguez, S. Cotillas, Removal of organochlorine pollutants from DNAPL-saturated groundwater using electrolysis with MMO anodes, Chem. Eng. J. (2024) 486.
[32] S. Cotillas, E. Lacasa, C. Sáez, P. Cañizares, M.A. Rodrigo, Disinfection of urine by conductive-diamond electrochemical oxidation, Appl. Catal. B: Environ. 229 (2018) 63–70.
[33] Á. Moratalla, S. Cotillas, E. Lacasa, P. Cañizares, M.A. Rodrigo, C. Sáez, Electrochemical technologies to decrease the chemical risk of hospital wastewater and urine, Molecules. 26 (2021).
[34] M. Herraiz-Carboné, S. Cotillas, E. Lacasa, Á. Moratalla, P. Cañizares, M. A. Rodrigo, C. Sáez, Improving the biodegradability of hospital urines polluted with chloramphenicol by the application of electrochemical oxidation, Sci. Total. Environ. 725 (2020).
[35] L.A. Goulart, A. Moratalla, P. Cañizares, M.R.V. Lanza, C. Sáez, M.A. Rodrigo, High levofloxacin removal in the treatment of synthetic human urine using Ti/MMO/ZnO photo-electrocatalyst, J. Environ. Chem. Eng. 10 (2022) 107317.
[36] S. Cotillas, E. Lacasa, C. Sáez, P. Cañizares, M.A. Rodrigo, Removal of pharmaceuticals from the urine of polymedicated patients: a first approach, Chem. Eng. J. 331 (2018) 606–614.
[37] S. Cotillas, E. Lacasa, C. Sáez, P. Cañizares, M.A. Rodrigo, Electrolytic and electro-irradiated technologies for the removal of chloramphenicol in synthetic urine with diamond anodes, Water. Res. 128 (2018) 383–392.
[38] I.M. Kolthoff, E.M. Carr, Volumetric determination of persulfate in the presence of organic substances, Anal. Chem. 25 (1953) 298–301.
[39] H. Sanderson, D.J. Johnson, C.J. Wilson, R.A. Brain, K.R. Solomon, Probabilistic hazard assessment of environmentally occurring pharmaceuticals toxicity to fish, daphnids and algae by ECOSAR screening, Toxicol. Lett. 144 (2003) 383–395.

[40] P. Cañizares, C. Sáez, A. Sánchez-Carretero, M.A. Rodrigo, Synthesis of novel oxidants by electrochemical technology, J. Appl. Electrochem. 39 (2009) 2143–2149.
[41] B. Marselli, J. Garcia-Gomez, P.A. Michaud, M.A. Rodrigo, C. Comninellis, Electrogeneration of hydroxyl radicals on boron-doped diamond electrodes, J. Electrochem. Soc. 150 (2003) D79–D83.
[42] P. Saha, J. Wang, Y. Zhou, L. Carlucci, A.W. Jeremiasse, H.H.M. Rijnaarts, H. Bruning, Effect of electrolyte composition on electrochemical oxidation: active sulfate formation, benzotriazole degradation, and chlorinated by-products distribution, Env.. Res 211 (2022) 113057.
[43] C.A. Martínez-Huitle, M.A. Rodrigo, I. Sirés, O. Scialdone, A critical review on latest innovations and future challenges of electrochemical technology for the abatement of organics in water, Appl. Catal. B: Environ. 328 (2023) 122430.
[44] M.A.Q. Alfaro, S. Ferro, C.A. Martínez-Huitle, Y.M.J.J.o.t.B.C.S. Vong, Boron doped diamond electrode for the wastewater treatment, 17 (2006) 227–236.
[45] M. Herraiz-Carboné, A. Santos, A. Hayat, C.M. Domínguez, S. Cotillas, Remediation of groundwater polluted with lindane production wastes by conductive-diamond electrochemical oxidation, Sci. Total. Environ. 926 (2024) 171848.
[46] S.D. Richardson, Disinfection by-products and other emerging contaminants in drinking water, TrAC Trends Anal. Chem. 22 (2003) 666–684.
[47] M. Herraiz-Carboné, E. Lacasa, S. Cotillas, M. Vasileva, P. Cañizares, M.A. Rodrigo, C. Sáez, The role of chloramines on the electrodisinfection of Klebsiella pneumoniae in hospital urines, Chem. Eng. J. 409 (2021) 128253.
[48] G. Nair, B. Soni, M. Shah, A comprehensive review on electro-oxidation and its types for wastewater treatment, Groundw. Sustain. Dev. 23 (2023) 100980.
[49] J. Guo, C. Ding, W. Gan, P. Chen, Y. Lu, J. Li, R. Chen, M. Zhang, Z. Sun, High-activity black phosphorus quantum dots/Au/TiO_2 ternary heterojunction for efficient levofloxacin removal: pathways, toxicity assessment, mechanism and DFT calculations, Sep. Purif. Technol. (2023) 307.
[50] C. Ding, Y. Lu, J. Guo, W. Gan, S. Qi, Z. Yin, M. Zhang, Z. Sun, Internal electric field-mediated sulfur vacancies-modified-In_2S_3/TiO_2 thin-film heterojunctions as a photocatalyst for peroxymonosulfate activation: density functional theory calculations, levofloxacin hydrochloride degradation pathways and toxicity of intermediates, Chem. Eng. J. (2022) 450.
[51] X. Chen, Y. Li, J. Hu, Y. Liang, B. Yuan, F. Yu, Y. Liu, X. Zheng, W. Yu, Ethylcellulose encapsulated material for potassium ferrate slow-release to degrade levofloxacin: degradation performance, mechanisms, and toxicity assessment, J. Environ. Chem. Eng. (2025) 13.
[52] A. United States Environmental Protection, Globally Harmonized System of Classification and Labelling of Chemicals (GHS): Chemical Hazard Classification and Labeling: Comparison of OPP Requirements and the GHS, United States Environmental Protection Agency, 2012, pp. 1–22.
[53] P. Guo, X. Hu, Co, Fe co-doped g-C_3N_4 composites as peroxymonosulfate activators under visible light irradiation for levofloxacin degradation: characterization, performance and synergy mechanism, Colloids Surf. Physicochem. Eng. Asp (2022) 648.
[54] Y. Gong, J. Li, Y. Zhang, M. Zhang, X. Tian, A. Wang, Partial degradation of levofloxacin for biodegradability improvement by electro-Fenton process using an activated carbon fiber felt cathode, J. Hazard. Mater. 304 (2016) 320–328.
[55] X.-Y. Lv, G.-P. Jin, D.-K. Yuan, Y.-F. Ding, P.-X. Long, Improving generation of H_2O_2 and •OH at copper hexacyanocobaltate/graphene/ITO composite electrode for degradation of levofloxacin in photo-electro-Fenton process, Environ. Sci. Pollut. Res. 28 (2021) 17636–17647.